EX. I

A monomeric red fluorescent protein

Robert E. Campbell*, Oded Tour*†, Amy E. Palmer*, Paul A. Steinbach*†, Geoffrey S. Baird*, David A. Zacharias*†‡, and Roger Y. Tsien*†§¶

Departments of *Pharmacology and §Chemistry and Biochemistry, and †Howard Hughes Medical Institute, University of California at San Diego, 9500 Gilman Drive, La Jolla, CA 92093

All coelenterate fluorescent proteins cloned to date display some form of quaternary structure, including the weak tendency of *Aequorea* green fluorescent protein (GFP) to dimerize, the obligate dimerization of *Renilla* GFP, and the obligate tetramerization of the red fluorescent protein from *Discosoma* (DsRed). Although the weak dimerization of *Aequorea* GFP has not impeded its acceptance as an indispensable tool of cell biology, the obligate tetramerization of DsRed has greatly hindered its use as a genetically encoded fusion tag. We present here the stepwise evolution of DsRed to a dimer and then either to a genetic fusion of two copies of the protein, i.e., a tandem dimer, or to a true monomer designated mRFP1 (monomeric red fluorescent protein). Each subunit interface was disrupted by insertion of arginines, which initially crippled the resulting protein, but red fluorescence could be rescued by random and directed mutagenesis totaling 17 substitutions in the dimer and 33 in mRFP1. Fusions of the gap junction protein connexin43 to mRFP1 formed fully functional junctions, whereas analogous fusions to the tetramer and dimer failed. Although mRFP1 has somewhat lower extinction coefficient, quantum yield, and photostability than DsRed, mRFP1 matures >10 times faster, so that it shows similar brightness in living cells. In addition, the excitation and emission peaks of mRFP1, 584 and 607 nm, are ≈25 nm red-shifted from DsRed, which should confer greater tissue penetration and spectral separation from autofluorescence and other fluorescent proteins.

The red fluorescent protein cloned from *Discosoma* coral (DsRed or drFP583) (1) holds great promise for biotechnology and cell biology as a spectrally distinct companion or substitute for the green fluorescent protein (GFP) from the *Aequorea* jellyfish (2). GFP and its blue, cyan, and yellow variants have found widespread use as genetically encoded indicators for tracking gene expression and protein localization and as donor/acceptor pairs for fluorescence resonance energy transfer (FRET). Extending the spectrum of available colors to red wavelengths would provide a distinct label for multicolor tracking of fusion proteins, and together with GFP (or a suitable variant) would provide a FRET donor/acceptor pair that should be superior to the currently preferred cyan/yellow pair (3). However, the evolution of DsRed from a scientific curiosity to a generally applicable and robust tool has been hampered by several critical problems, including a slow and incomplete maturation and obligate tetramerization (4). Most previous attempts to address the rate and/or extent of maturation of DsRed (5, 6), including the commercially available DsRed2 (CLONTECH), have provided only modest improvements. However, an engineered variant of DsRed, known as T1 (see Fig. 1A), has recently become available and effectively solved the problem of the slow maturation (7). Another approach to overcoming these shortcomings has been to continue the search for DsRed homologues in sea coral and anemone, an approach that has yielded several red-shifted tetramers (8, 9). The more fundamental problem of tetramerization, however, has yet to be overcome. The only published progress toward decreasing the oligomeric state of a red fluorescent protein involved an engineered DsRed homologue, commercially available as HcRed1 (CLONTECH), which was converted to a dimer with a single interface mutation (10). Although HcRed1 has the additional benefit of being 35 nm

red-shifted from DsRed, it is limited by a rather low extinction coefficient ($20,000 \text{ M}^{-1}\cdot\text{cm}^{-1}$) and quantum yield (0.015) (11).

A variety of techniques have confirmed that DsRed is an obligate tetramer *in vitro* (4, 12) and in living cells (4), but for the researcher who wants to image the subcellular localization of a red fluorescent chimera the question remains to what extent will fusing tetrameric DsRed to the protein of interest affect the location and function of the latter? There have been several published reports (3, 13), and many unpublished anecdotal communications, in which DsRed chimeras have been described as forming intracellular aggregates. The consensus is that a monomeric form of DsRed will be essential if it is to ever reach its full potential as a genetically encoded red fluorescent tag (14). In this article we report the directed evolution and preliminary characterization of a monomeric red fluorescent protein (mRFP). Although further refinements of this protein are desirable and likely, it already provides an independent alternative to GFP in the construction of fluorescently tagged fusion proteins.

Materials and Methods

Mutagenesis and Screening. DsRed, amplified from vector pDsRed-N1 (CLONTECH) or T1 (provided by B. S. Glick, Univ. of Chicago) in pRSET_B (Invitrogen) (4), was used as the template for introduction of the I125R mutant with the Quick-Change kit (Stratagene). Error-prone PCR was performed as described (15). Semirandom mutations at multiple distant locations were introduced by overlap extension PCR (16) with multiple fragments. Briefly, 2–4 pairs of sense and antisense oligonucleotides (Invitrogen or GenBase, San Diego), with semidegenerate codons at positions of interest, were used for PCR amplification of the DsRed template with Pfu polymerase (Stratagene) in individual reactions. The resulting overlapping fragments were gel-purified (Qiagen, Valencia, CA) and recombined by overlap extension PCR with Pfu or *Taq* polymerase (Roche Molecular Biochemicals). Full-length genes were digested with *Bam*HI/*Eco*RI (New England Biolabs) and ligated into pRSET_B with T4 ligase (New England Biolabs). Chemically competent *Escherichia coli* JM109(DE3) were transformed and grown overnight on LB/agar at 37°C and maintained at room temperature for weeks if necessary. LB/agar plates were screened by using a cooled charge-coupled device camera as described (17), and the digital images were processed with METAMORPH software (Universal Imaging, West Chester, PA). All screening was done with 470-nm (40-nm bandwidth), 540-nm (30-nm bandwidth), or 560-nm (40-nm bandwidth) excitation filters and 530-nm (40-nm bandwidth), 575-nm (long pass), or 610-nm (long pass) emission filters. Colonies of interest were

---

Fig. 1. Graphical representation of the tetramer, dimer, and monomer of DsRed based on the x-ray crystal structure of DsRed (21). Residues 1–5 were not observed in the crystal structure (Protein Data Bank identification 1G7K) but have been arbitrarily appended for the sake of representation. The DsRed chromophore is represented in red, and the four chains of the dimer are labeled following the convention of Yarbrough et al. (21). (*A*) The tetramer of DsRed with all residues mutated in T1 indicated in green for external residues and blue for those internal to the β-barrel. (*B*) The AC dimer of DsRed with all mutations present in dimer2 represented as in *A* and the intersubunit linker present in tdimer2(12) shown as a dotted line. (*C*) The monomer of DsRed with all mutations present in mRFP1 represented as in *A*. This figure was produced with MOLSCRIPT (27).

cultured overnight in 2 ml of LB supplemented with ampicillin. Bacteria were pelleted by centrifugation and imaged to ensure that the protein was expressed well in culture. For fast maturing proteins a fraction of the cell pellet was extracted with B-per II (Pierce), and complete spectra were obtained. DNA was purified from the remaining pellet by QIAprep spin column (Qiagen) and submitted for sequencing. To determine the oligomeric state of DsRed mutants, a single colony of *E. coli* was restreaked on LB/agar and allowed to mature at room temperature. After 2 days to 2 weeks the bacteria were scraped from the plate, extracted with B-per II, and analyzed (not boiled) by SDS/PAGE (BioRad), and the gel was imaged with a digital camera.

Construction of Tandem Dimers and Constructs for Mammalian Cell Expression. To construct tandem dimers, dimer2 in pRSET$_B$ was amplified in two separate PCRs. In the first reaction, a 5' *Bam*HI and a 3' *Sph*I site were introduced, whereas in the second reaction a 5' *Sac*I and a 3' *Eco*RI site were introduced. The construct was assembled in a four-part ligation containing the digested dimer2 genes, a synthetic linker with phosphorylated sticky ends, and digested pRSET$_B$. The linkers used included a nine-residue linker (RMGTGSGQL), a 12-residue linker (GH-GTGSTGSGSS), a 13-residue linker (RMGSTSGSTKGQL), and a 22-residue linker (RMGSTSGSGKPGSGEGSTKGQL). For expression in mammalian cells, DsRed variants were amplified from pRSET$_B$ with a 5' primer that encoded a *Kpn*I restriction site and a Kozak sequence. The PCR product was digested, ligated into pcDNA3, and used to transform *E. coli* DH5α. To construct the connexin43 (Cx43) DsRed fusions, Cx43 was first amplified with a 3' primer encoding a seven-residue linker ending in a *Bam*HI site. The construct was assembled in a three-part ligation containing *Kpn*I/*Bam*HI-digested Cx43, *Bam*HI/*Eco*RI-digested enhanced GFP (EGFP), and digested pcDNA3. For all other fusion proteins (Cx43-T1, -dimer2, -tdimer2(12), and -mRFP1) the gene for the fluorescent protein was ligated into the *Bam*HI/*Eco*RI digested Cx43-GFP vector.

Protein Production and Characterization. DsRed variants were expressed as described (17). All proteins were purified by Ni-NTA chromatography (Qiagen) and dialyzed into 10 mM Tris, pH 7.5 or PBS supplemented with 1 mM EDTA. All biochemical characterization experiments, including the determination of extinction coefficients, analytical ultracentrifugation, and absorption and fluorescence spectra, were performed as described (4). The maturation time course and pH sensitivity were determined on a Safire 96-well plate reader with monochromators (TECAN, Männedorf, Switzerland). All photobleaching measurements were performed in microdroplets under paraffin oil (4) with a Zeiss Axiovert 35 fluorescence microscope equipped with a ×40 objective and a 540-nm (25-nm bandpass) excitation filter that delivered 4.5 W/cm² of light.

Mammalian Cell Imaging and Microinjection. HeLa cells were transfected with DsRed variants or Cx43-DsRed fusions in pcDNA3 through the use of Fugene 6 (Roche Diagnostics). Transfected cells were grown for 12 h to 2 days in DMEM at 37°C before imaging with a Zeiss Axiovert 35 fluorescence microscope with cells in glucose-supplemented Hanks' balanced salt solution at room temperature. Individual cells expressing Cx43 fused to a DsRed variant, or contacting nontransfected cells for control experiments, were microinjected with a 2.5% solution of lucifer yellow (Molecular Probes). Images were acquired and processed with the METAFLUOR software package.

Results

Evolution of a Dimer of DsRed. Our basic strategy for decreasing the oligomeric state of DsRed was to replace key dimer interface

Table 1. Summary of spectroscopic data

	Excitation maximum, nm	Emission maximum, nm	Extinction coefficient per chain, $M^{-1} \cdot cm^{-1}$	Fluorescence quantum yield	Rate of photobleach relative to EGFP		pKa	$t_{0.5}$ for maturation at 37°C
					Fast	Slow		
DsRed	558	583	57,000	0.79	0.23	0.022	4.7	~10 h
T1	555	584	35,000	0.51	0.15	0.012	4.8	<1 h
dimer2	552	579	60,000	0.69	0.36	0.018	4.9	~2 h
tdimer2(12)	552	579	120,000	0.68	0.31	0.014	4.8	~2 h
mRFP1	584	607	44,000	0.25	7.2	0.16	4.5	<1 h

residues with arginine. When the targeted residue interacts with the identical residue of the dimer partner through symmetry, the high energetic cost of placing two positive charges in close proximity should disrupt the interaction. Such a strategy disrupted the weak tendency of *Aequorea* GFP to dimerize, without any deleterious effects on GFP maturation or brightness (18). Initial attempts to break apart the DsRed AC interface (see Fig. 1*A*) with the single mutations T147R, H162R, and F224R consistently gave nonfluorescent proteins (19). The AB interface, however, proved somewhat less resilient and could be broken with the single mutation I125R to give a poorly red fluorescent dimer that suffered from an increased green component and required more than 10 days to fully mature (19).

To reconstitute the red fluorescence of DsRed–I125R, we subjected the protein to iterative cycles of evolution. Within each cycle, the protein was randomly mutagenized to find sequence locations that affected the maturation and brightness of the protein, and then expanded libraries of mutations at those positions were created and recombined to find optimal permutations (see Fig. 6, which is published as supporting information on the PNAS web site, www.PNAS.org). This strategy resulted in modest progress toward rescuing DsRed–I125R, but our focus quickly turned to the fast tetramer T1 (7) when we discovered that introduction of the I125R mutation into this protein resulted in a dimer that matured in only a few days, similar to our best DsRed dimers at that time. Targeting those positions that had helped rescue DsRed–I125R resulted in dramatic improvements in our first-generation library. Continuing with our directed evolution strategy for a total of four generations (see additional *Discussion*, Table 2, Table 3, and primer lists, which are published as supporting information on the PNAS web site) we eventually produced our best dimeric variant, which we have designated dimer2 (Fig. 1*B*). Of the 17 mutations in dimer2, eight are internal to the β-barrel (N42Q, V44A, V71A, F118L, K163Q, S179T, S197T, and T217S), three are the aggregation-reducing mutations (7, 20) found in T1 (R2A, K5E, and N6D), two are AB interface mutations (I125R and V127T), and four are miscellaneous surface mutations (T21S, H41T, C117T, and S131P).

Construction of a Tandem Dimer of DsRed. Based on our early results, it seemed as though engineering a true monomer of DsRed might be impossible and therefore we pursued an alternate approach. The basic strategy was to fuse two copies of our best AC dimer with a polypeptide linker such that the critical dimer interactions could be satisfied through intramolecular contacts with the tandem partner encoded within the same polypeptide. Based on the crystal structure of the DsRed tetramer (21, 22) a 10- to 20-residue linker could extend from the C terminus of the A subunit to the N terminus of the C subunit (~30 Å, Fig. 1*B*), but not to the N terminus of the B subunit (>70 Å). With our optimized dimer2 we constructed a series of tandem constructs with linkers of varying lengths (9, 12, 13, or 22 aa) and a sequence similar to a known protease-resistant

linker (23). Of these four, only the tandem construct with the nine-residue linker was notable for its somewhat slower maturation. The other three constructs were practically indistinguishable, and the tandem construct with the 12-residue linker, designated tdimer2(12), is currently our preferred construct because it has the shortest linker. As expected, dimer2 and tdimer2(12) have identical excitation and emission maximum and quantum yields (see Table 1). However, the extinction coefficient of tdimer2(12) is twice that of dimer2 because of the presence of two equally absorbing chromophores per polypeptide chain.

Evolution of a Monomer of DsRed. With the hope that our improved dimers of DsRed would better tolerate disruption of the remaining interface, we constructed libraries in which AC interface-breaking mutations were incorporated into our best dimers. Our first such library targeted nine different positions, including two key AC interface residues, H162 and A164, which were forced to be either lysine or arginine. The brightest colonies from this library were difficult to distinguish from the background red fluorescence of the *E. coli* colonies even after prolonged imaging with a digital camera. Suspect colonies were restreaked on LB/agar and allowed to mature at room temperature for 2 weeks, and a crude protein preparation was analyzed by SDS/PAGE. Imaging of the gel revealed a single faint band consistent with the expected mass of the monomer and thus mRFP0.1 was identified. Continuing with our directed evolution strategy for six additional generations (see Tables 2 and 3 and primer lists) resulted in drastic improvements in the brightness and rate of maturation. The final clone, designated mRFP1, contains a total of 33 mutations (Fig. 1*C*) relative to DsRed of which 13 are internal to the β-barrel (N42Q, V44A, V71A, K83L, F124L, L150M, K163M, V175A, F177V, S179T, V195T, S197I, and T217A). Of the 20 remaining external mutations, three are the aggregation-reducing mutations from T1 (R2A, K5E, and N6D), three are AB interface mutations (I125R, V127T, and I180T), ten are AC interface mutations (R153E, H162K, A164R, L174D, Y192A, Y194K, H222S, L223T, F224G, and L225A), and four are additional beneficial mutations (T21S, H41T, C117E, and V156A).

Characterization of dimer2, tdimer2(12), and mRFP1. Our initial evidence for the monomeric structure of mRFP1 and its precursors was based on results with SDS/PAGE (see Fig. 7, which is published as supporting information on the PNAS web site) and the lack of FRET between the green and red fluorescent components in early generations. Thus analytical equilibrium ultracentrifugation was performed on DsRed, dimer2, and mRFP0.5a (an evolutionary precursor to mRFP1), and the results confirmed the expected tetramer, dimer, and monomer sizes (Fig. 2). DsRed, T1, and dimer2 (Fig. 3 *A–C*) all have a fluorescent component that contributes at 475–486 nm to the excitation spectra caused by FRET between oligomeric partners (4). In T1 (Fig. 3*B*) this peak is quite pronounced, but in dimer2
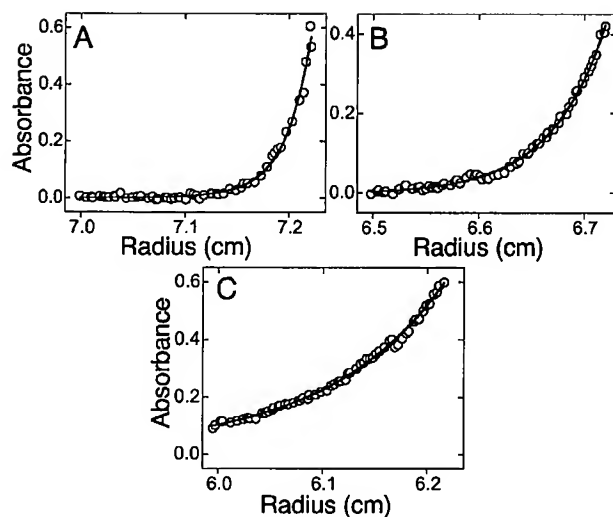
Fig. 2. Analytical ultracentrifugation analysis of DsRed, dimer2, and mRFP0.5a. The equilibrium radial absorbance profiles at 20,000 rpm were modeled with a theoretical curve that allowed only the molecular weight to vary. (A) The DsRed absorbance profile was best fit with an apparent molecular mass of 120 kDa, consistent with a tetramer. (B) The dimer2 absorbance profile was best fit with an apparent mass weight of 60 kDa, consistent with a dimer. (C) The mRFP0.5a absorbance profile was best fit with an apparent molecular mass of 32 kDa, consistent with a monomer containing an N-terminal polyhistidine affinity tag.

(Fig. 3C), any excitation shoulder near 480 nm is almost obscured by the 5-nm blue-shifted excitation peak. The 25-nm red-shifted monomeric mRFP1 (Fig. 3D) also has a peak at 503 nm in the absorption spectra, but in contrast to the other variants, this species is nonfluorescent and therefore does not show up in the excitation spectrum collected at any emission wavelength. The green component of all DsRed variants may be caused by a fraction of the protein that never matures beyond the green intermediate (4, 24) or is trapped in a dead end product such as a nonproductive trans conformation for the F65–Q66 peptide bond (22). In either case it is not clear why this species would be nonfluorescent in mRFP1. The large discrepancy in amplitude
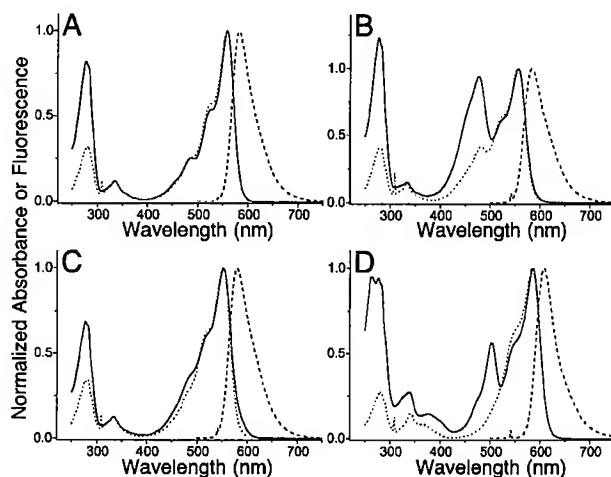

Fig. 3. Fluorescence and absorption spectra of DsRed (A), T1 (B), dimer2 and tdimer2(12) (C), and mRFP1 (D). The absorbance spectrum is shown with a solid line, the excitation with a dotted line, and the emission with a dashed line.
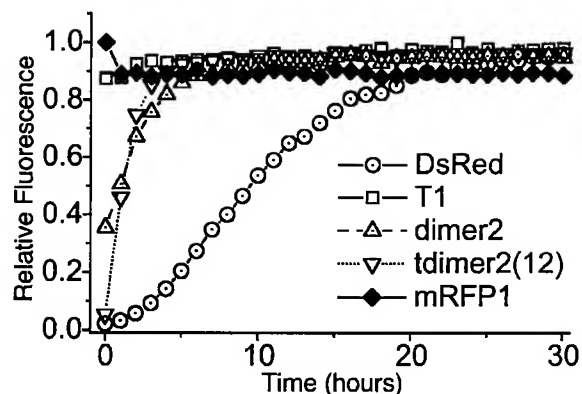

Fig. 4. Maturation of red fluorescence for DsRed, T1, dimer2, tdimer2(12), and mRFP1. Log-phase cultures of E. coli expressing the construct of interest were rapidly purified at 4°C, and beginning at 2 h postharvest their maturation at 37°C was monitored. The initial decrease in mRFP1 fluorescence is attributed to a slight quenching on warming from 4°C to 37°C.

between the 480-nm absorption and excitation peaks in T1 suggests that the corresponding species in T1 also has a very low average quantum yield.

All red fluorescent proteins displayed double exponential kinetics for photobleaching, suggesting a two-step process, whereas EGFP under similar conditions bleached with very nearly single exponential kinetics. Table 1 gives the rates of the fast and slow components of the red proteins' bleaching, normalized to the rate for EGFP bleaching with an equivalent photon flux at EGFP's absorbance maximum. Our bleaching measurements of DsRed and EGFP are in good absolute agreement with previous reports (for fuller discussion see additional *Discussion* and Table 4, which are published as supporting information on the PNAS web site).

As shown in Fig. 4, the rate of maturation of dimer2, tdimer2(12), and mRFP1 is greatly accelerated over that of DsRed although only mRFP1 matures at least as quickly as T1. Based on our data at 37°C, we estimate the $t_{0.5}$ for maturation of mRFP1 and T1 is less than 1 h, consistent with the 0.7 h previously reported for T1 (7). *E. coli* colonies expressing either dimer2 or mRFP1 display similar or brighter levels of fluorescence to those expressing T1 after overnight incubation at 37°C (see Fig. 8, which is published as supporting information on the PNAS web site). The improved brightness of dimer2 may be making up for its slower maturation. For mRFP1, which is less bright than T1, we speculate that a higher folding efficiency is the compensating factor.

Expression of dimer2, tdimer2(12), and mRFP1 in Mammalian Cells. Although we suspected that we had evolved relatively robust red fluorescent proteins, it was not known whether they were suitable for expression in mammalian cells. Therefore dimer2, tdimer2(12), and mRFP1 were expressed in transiently transfected HeLa cells. Within 12 h the cells displayed strong red fluorescence evenly distributed throughout the nucleus and cytoplasm (data not shown). This result prompted us to explore a series of fusion constructs, using the gap junction protein Cx43, which could demonstrate the advantage of a mRFP. A series of constructs consisting of Cx43 fused to either GFP, T1, dimer2, tdimer2(12), or mRFP1 were expressed in HeLa cells, which do not express endogenous connexins. As previously reported (13) the Cx43–GFP fusion protein was properly trafficked to the membrane and was assembled into functional gap junctions, whereas the Cx43–DsRed tetramer [T1 in this work, DsRed in previous work (13)] consistently formed perinuclear localized
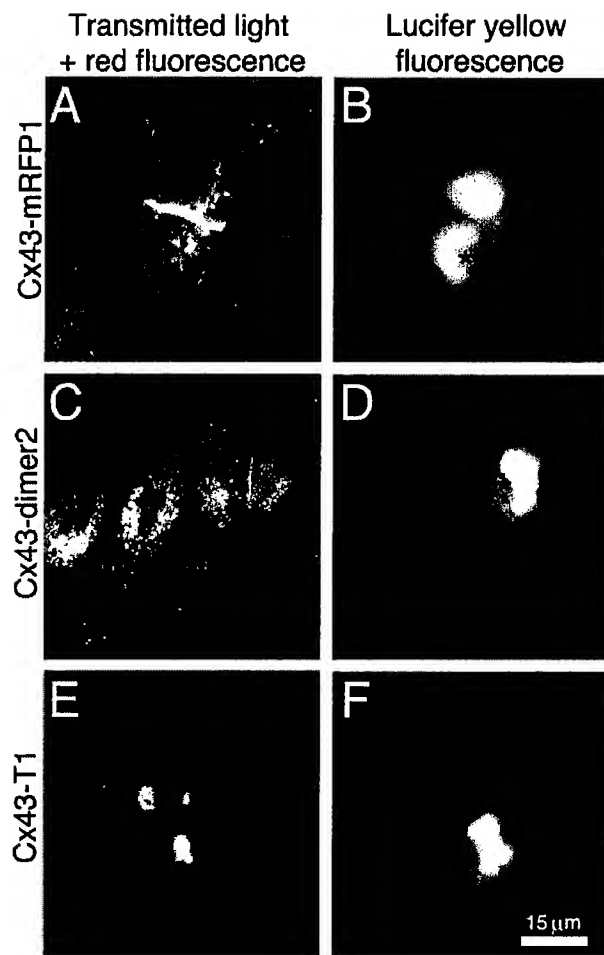
Transmitted light + red fluorescence

Lucifer yellow fluorescence

Fig. 5. HeLa cells expressing Cx43 fused with T1, dimer2, or mRFP1. (A, C, and E) Images were acquired with excitation at 568 nm (55 nm bandwidth) and emission at 653 nm (95 nm bandwidth) with additional transmitted light. Lucifer yellow fluorescence (B, D, and F) was acquired with excitation at 425 nm (45 nm bandpass) and emission at 535 nm (55 nm bandpass). (A) Two contacting cells transfected with Cx43-mRFP1 and connected by a single large gap junction. (B) One cell is microinjected with lucifer yellow at the point indicated by * and the dye quickly passes (1–2 s) to the adjacent cell. (C) Four neighboring cells transfected with Cx43-dimer2. The bright line between the two rightmost cells is the result of having two fluorescent membranes in contact and is not a gap junction. (D) As was observed about one-third of the time, microinjected dye is slowly passed to an adjacent cell. (E) Two adjacent cells transfected with Cx43-T1 and displaying the typical perinuclear localized aggregation. (F) No dye passed between neighboring cells.

red fluorescent aggregates. Both Cx43–tdimer2(12) and Cx43–dimer2 were properly trafficked to the membrane although neither construct formed visible gap junctions. In contrast, the Cx43–mRFP1 construct behaved identically to Cx43–GFP and many red gap junctions were observed. Transfected cells were microinjected with lucifer yellow to assess the functionality of the gap junctions (see Fig. 5 and Table 5, which is published as supporting information on the PNAS web site). The Cx43–mRFP1 gap junctions rapidly and reliably passed dye, whereas neither Cx43-T1-transfected cells nor nontransfected cells passed dye. Interestingly, both Cx43–dimer2 and Cx43–tdimer2(12) constructs slowly passed dye to a contacting transfected neighbor about one-third of the time. This apparently "gap junction independent" dye transfer may indicate that the

plasma membrane contains functional connexon channels that are unable to assemble into gap junctions plaques because of steric crowding of the fused dimer2 or tdimer2(12). Alternatively, dye transfer may be caused by gap junctions smaller than the resolution of our camera.

Discussion

Initially, we were faced with the decision of how to efficiently construct and screen libraries of DsRed mutants such that we could direct the evolution of tetrameric DsRed toward a mRFP. Ultimately the best solution was to take the semirational approach of breaking the dimer interfaces in a stepwise fashion (first AB then AC) and undertaking a directed evolution strategy to rescue the red fluorescence. This combination of targeted and random mutagenesis successfully directed the evolution of DsRed from the poorly fluorescent dimer T1-I125R to the monomeric mRFP1 in eight generations. In retrospect, breaking up the tetramer was not the barrier to the discovery of mRFP1; the challenge was to find the correct combination of many mutations to rescue the red fluorescence in the crippled dimers and monomers.

There are likely several mechanisms by which mutations in dimer2 and mRFP1 have contributed to rescuing the red fluorescence. Although one mechanism probably involves improving the folding efficiency or stability of the monomer, the most important factor is undoubtedly the effect on the rate-determining conversion from the "GFP-like" intermediate to the DsRed chromophore (21, 24). Without crystal structures of immature and mature forms of each mutant, little can be said about the subtle effects each individual substitution may or may not have on this poorly understood transformation. However, all of the mutations discovered in this research and many of those previously reported (4, 25) appear to cluster into three "hotspots." The first of these hotspots is found in the plane of the chromophore (when oriented as in Fig. 1C) and is defined by N42, V44, and the Q66 side chain of the chromophore. The mutations N42Q and V44A originated in T1 where they bestowed the tetramer with a greatly improved maturation time (7), possibly by positioning Q66 in a conformation that promotes the oxidation that transforms the green intermediate into the red chromophore. Despite the extensive random and directed mutagenesis in this study, better mutations at or near these positions were never identified, suggesting that these are nearly optimal replacements. The second hotspot is just above the plane of the chromophore, centered on the side chain K163 and influenced by V175, F177, and possibly I161 (6). In the crystal structure of DsRed, the phenolate anion of the chromophore is stabilized by a salt bridge with the primary amine of K163 (22). Neither the K163Q mutation in dimer2 nor the K163M mutation in mRFP1 can participate in a salt bridge and therefore the polarization of the chromophore may be significantly different in these variants. The third and most sensitive hotspot is found just below the plane of the chromophore and is centered on the side chains of K70 and the adjacent S197 and T217. Conservative mutations such as K70R, S197T, and T217S had dramatic effects on the fluorescent properties of DsRed mutants and were critical intermediate steps toward mRFP1. Additionally, many of the beneficial mutations in hydrophobic pockets of mRFP1, such as V71A and L150M, are near this region and may be influencing the chromophore through subtle packing rearrangements that are mediated through this polar microenvironment. Interestingly, the S197I mutation of mRFP1 is structurally analogous to the T203I mutation in the sapphire variant of GFP, also known as H9-40 (2), where it is believed to destabilize the anionic form of the chromophore. Considering that in mRFP1 the phenolate oxygen is sandwiched between this same replacement and the nonpolar K163M mutation, the overall effect should be to shift electron density away from the phenolic anion. This repolarization may

make the imidazolinone ring more electron rich and thereby promote oxidation of the adjacent Q66 main-chain atoms to form the acylimine of the extended DsRed chromophore (24). The hydrophobic environment around the phenolic oxygen, which is located in close proximity to the AC dimer interface, may also serve to isolate and stabilize the critical hydrogen bond to S146 and thus compensate for the loss of former AC interface interactions. Fortunately, the pKa of the chromophore remains low, <5.0 (Table 1), despite these alterations in its immediate environment.

The monomeric mRFP1 simultaneously overcomes the three critical problems associated with the wild-type tetramer of DsRed (4). Specifically mRFP1 is a monomer, it matures rapidly, and it has minimal emission when excited at wavelengths optimal for GFP. These features make mRFP1 the most suitable red fluorescent protein for the construction of fusion proteins and multicolor labeling in combination with GFP. As we have demonstrated with the gap junction-forming protein Cx43, mRFP1 fusion proteins are functional and trafficked identically to their GFP analogues. Unfortunately, mRFP1 is not yet ideal for all applications because its fluorescence quantum yield and extinction coefficient (0.25 and 44,000 $M^{-1}\cdot cm^{-1}$, respectively) are significantly lower than for other DsRed variants (Table 1) although much higher than HcRed1 (0.015 and 20,000 $M^{-1}\cdot cm^{-1}$, respectively) (11). Also, mRFP1 photobleaches about 10-fold more easily than other DsRed variants, although its photostability is still comparable to that for Aequorea EGFP (26). Although the low extinction coefficient is attributable to the significant fraction of the protein that remains trapped as a nonfluorescent green species, the decreased fluorescence quantum yield and increased photobleaching quantum yield may reflect imperfect shielding of the fluorophore by the surrounding cylindrical shell of β-strands. The monomer has only one layer of β-strands separating the fluorophore from solvent and

oxygen, whereas the tetramer subunits should give each other additional protection. Perhaps tight tetramerization of wild-type coral proteins evolved to maximize thermotolerance or photostability under intense tropical sunlight; the progressive decrease in oligomerization going from corals and corallimorphs (obligate tetramer) to Renilla (southern U.S. waters, obligate dimer) and Aequorea (Pacific Northwest, weak dimer) correlates with decreasing habitat temperature and intensity of daylight.

The extinction coefficient and fluorescence quantum yield limit the brightness of fully mature mRFP1 to approximately 25% of DsRed, although for most imaging experiments this limit will be more than compensated for by the greater than 10-fold decrease in maturation time for mRFP1. However these factors do render mRFP1 currently nonoptimal for the construction of FRET-based sensors (unpublished observations). An interim solution is to use the nonoligomerizing tdimer2(12), which is very bright and displays FRET with all variants of Aequorea GFP (unpublished observations). We expect that yet more desirable mRFP variants with higher quantum yield and diminished green component will be engineered. Similar multistep evolutionary strategies, involving many rounds of evolution with few mutational steps per cycle, are likely to be profitable in converting other oligomeric fluorescent proteins into monomers.

1. Matz, M. V., Fradkov, A. F., Labas, Y. A., Savitsky, A. P., Zaraisky, A. G., Markelov, M. L. & Lukyanov, S. A. (1999) Nat. Biotechnol. 17, 969–973.
2. Tsien, R. Y. (1998) Annu. Rev. Biochem. 67, 509–544.
3. Mizuno, H., Sawano, A., Eli, P., Hama, H. & Miyawaki, A. (2001) Biochemistry 40, 2502–2510.
4. Baird, G. S., Zacharias, D. A. & Tsien, R. Y. (2000) Proc. Natl. Acad. Sci. USA 97, 11984–11989.
5. Verkhusha, V. V., Otsuna, H., Awasaki, T., Oda, H., Tsukita, S. & Ito, K. (2001) J. Biol. Chem. 276, 29621–29624.
6. Terskikh, A. V., Fradkov, A. F., Zaraisky, A. G., Kajava, A. V. & Angres, B. (2002) J. Biol. Chem. 277, 7633–7636.
7. Bevis, B. J. & Glick, B. S. (2002) Nat. Biotechnol. 20, 83–87.
8. Fradkov, A. F., Chen, Y., Ding, L., Barsova, E. V., Matz, M. V. & Lukyanov, S. A. (2000) FEBS Lett. 479, 127–130.
9. Lukyanov, K. A., Fradkov, A. F., Gurskaya, N. G., Matz, M. V., Labas, Y. A., Savitsky, A. P., Markelov, M. L., Zaraisky, A. G., Zhao, X., Fang, Y., et al. (2000) J. Biol. Chem. 275, 25879–25882.
10. Gurskaya, N. G., Fradkov, A. F., Terskikh, A., Matz, M. V., Labas, Y. A., Martynov, V. I., Yanushevich, Y. G., Lukyanov, K. A. & Lukyanov, S. A. (2001) FEBS Lett. 507, 16–20.
11. CLONTECH Laboratories (2002) Living Colors User Manual Vol. II: Red Fluorescent Protein (Becton Dickinson, Palo Alto, CA), p. 4.
12. Vrzheshch, P. V., Akovbian, N. A., Varfolomeyev, S. D. & Verkhusha, V. V. (2000) FEBS Lett. 487, 203–208.
13. Lauf, U., Lopez, P. & Falk, M. M. (2001) FEBS Lett. 498, 11–15.
14. Remington, S. J. (2002) Nat. Biotechnol. 20, 28–29.

15. Griesbeck, O., Baird, G. S., Campbell, R. E., Zacharias, D. A. & Tsien, R. Y. (2001) J. Biol. Chem. 276, 29188–29194.
16. Ho, S. N., Hunt, H. D., Horton, R. M., Pullen, J. K. & Pease, L. R. (1989) Gene 77, 51–59.
17. Baird, G. S., Zacharias, D. A. & Tsien, R. Y. (1999) Proc. Natl. Acad. Sci. USA 96, 11241–11246.
18. Zacharias, D. A., Violin, J. D., Newton, A. C. & Tsien, R. Y. (2002) Science 296, 913–916.
19. Baird, G. S. (2001) Ph.D. thesis (Univ. of California, San Diego).
20. Yanushevich, Y. G., Staroverov, D. B., Savitsky, A. P., Fradkov, A. F., Gurskaya, N. G., Bulina, M. E., Lukyanov, K. A. & Lukyanov, S. A. (2002) FEBS Lett. 511, 11–14.
21. Yarbrough, D., Wachter, R. M., Kallio, K., Matz, M. V. & Remington, S. J. (2001) Proc. Natl. Acad. Sci. USA 98, 462–467.
22. Wall, M. A., Socolich, M. & Ranganathan, R. (2000) Nat. Struct. Biol. 7, 1133–1138.
23. Whitlow, M., Bell, B. A., Feng, S. L., Filpula, D., Hardman, K. D., Hubert, S. L., Rollence, M. L., Wood, J. F., Schott, M. E., Milenic, D. E., et al. (1993) Protein Eng. 6, 989–995.
24. Gross, L. A., Baird, G. S., Hoffman, R. C., Baldridge, K. K. & Tsien, R. Y. (2000) Proc. Natl. Acad. Sci. USA 97, 11990–11995.
25. Wiehler, J., von Hummel, J. & Steipe, B. (2001) FEBS Lett. 487, 384–389.
26. Peterman, E. J. G., Brasselet, S. & Moerner, W. E. (1999) J. Phys. Chem. A 103, 10553–10560.
27. Kraulis, P. J. (1991) J. Appl. Crystallogr. 24, 946–950.